Contents lists available at ScienceDirect

Nuclear Inst. and Methods in Physics Research, A

Application of compact laser-driven accelerator X-ray sources for industrial imaging

J.-N. Gruse [a,*], M.J.V. Streeter [a,e], C. Thornton [b], C.D. Armstrong [b], C.D. Baird [b,d], N. Bourgeois [b], S. Cipiccia [f], O.J. Finlay [e], C.D. Gregory [b], Y. Katzir [b], N.C. Lopes [a,c], S.P.D. Mangles [a], Z. Najmudin [a], D. Neely [b], L.R. Pickard [g], K.D. Potter [h], P.P. Rajeev [b], D.R. Rusby [b,1], C.I.D. Underwood [d], J.M. Warnett [i], M.A. Williams [i], J.C. Wood [a,2], C.D. Murphy [d], C.M. Brenner [b], D.R. Symes [b,*]

[a] *John Adams Institute for Accelerator Science, Imperial College London, London, SW7 2BZ, UK*
[b] *Central Laser Facility, STFC Rutherford Appleton Laboratory, OX11 0QX, UK*
[c] *GoLP, IPFN, Instituto Superior Tecnico, U. Lisboa, Portugal*
[d] *York Plasma Institute, Department of Physics, University of York, York YO10 5DD, UK*
[e] *Physics Department, Lancaster University, Lancaster LA1 4YB, UK*
[f] *Diamond Light Source, Harwell Science & Innovation Campus, Oxfordshire OX11 0DE, UK*
[g] *National Composites Centre, Bristol and Bath Science Park, Feynman Way Central, Emersons Green, Bristol BS16 7FS, UK*
[h] *Advanced Composites Collaboration for Science and Innovation (ACCIS) University of Bristol, Bristol BS8 1TR, UK*
[i] *WMG, University of Warwick, Coventry CV4 7AL, UK*

ARTICLE INFO

ABSTRACT

X-rays generated by betatron oscillations of electrons in a laser-driven plasma accelerator were characterised and applied to imaging industrial samples. With a 125 TW laser, a low divergence beam with $5.2 \pm 1.7 \times 10^7$ photons mrad^{-2} per pulse was produced with a synchrotron spectrum with a critical energy of 14.6 ± 1.3 keV. Radiographs were obtained of a metrology test sample, battery electrodes, and a damage site in a composite material. These results demonstrate the suitability of the source for non-destructive evaluation applications. The potential for industrial implementation of plasma accelerators is discussed.

1. Introduction

Advances in industrial methods, such as additive manufacturing (AM), are enabling the fabrication of better and more complicated products than are achievable with traditional manufacturing. Environmental sustainability is a major incentive to develop less wasteful processes, new materials, and energy storage solutions. For example, many aircraft and automotive components are now produced using lightweight fibre reinforced composites to improve fuel efficiency. In parallel, the more widespread adoption of electric vehicles is driving investment and innovation in battery technologies. Rapid growth in these sectors means that in some cases demand is outstripping supply and there is a need for industry to increase productivity. Progress in manufacturing needs to be accompanied by improvements in the product inspection tools employed for metrology and quality control. X-ray computed tomography (XCT) is a powerful technique because it allows non-destructive evaluation (NDE) of the internal structure of dense objects. XCT is generally conducted using commercial x-ray tubes and linear accelerators but for some applications these sources are not able to simultaneously meet the demanding requirements on penetration, scan speed and spatial resolution.[3] Superior imaging capability can be achieved using synchrotron light sources, but these are national-scale facilities which are in high demand so that access for industrial inspection is limited.

We present an alternative compact, laser-based light source for industrial inspection that delivers extreme brightness, ultrashort x-ray pulses. This synchrotron source relies on a plasma-based electron accelerator driven by a high power laser (> 100 TW) [1]. The laser pulse is focused on to a gas target at a high intensity of 10^{19} W cm^{-2}, expelling on-axis electrons and creating ion cavities in its wake. Electrons injected into a cavity are subject to strong transverse and longitudinal electric fields (~ 100 GeV m^{-1}), accelerating to energies of
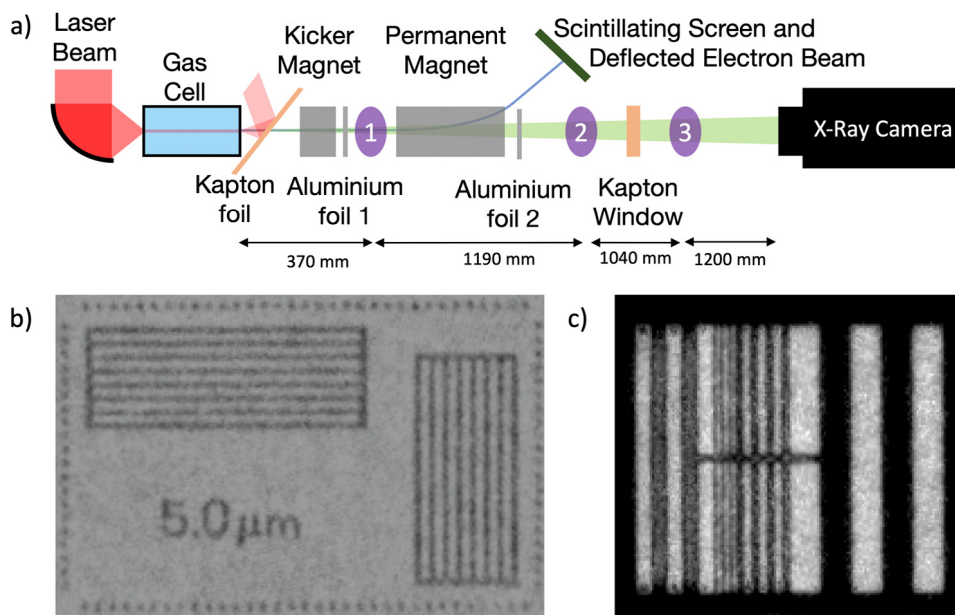

Fig. 1. (a) Schematic of the laser-betatron x-ray source including three sample positions (purple). The laser beam (red) is focused into a gas cell, in which electrons (blue) are accelerated, which then produce x-rays (green). Radiographs of: (b) resolution target (JIMA *RT RC-02*) with 5 μm line spacing, imaged at position 1 ($M = 10.2$); (c) resolution target (gold grid) with line spacing from left to right: 41.1 μm, 10.95 μm, 23.27 μm and 75.3 μm imaged at position 2 ($M = 2.2$). (For interpretation of the references to colour in this figure legend, the reader is referred to the web version of this article.)

multiple GeV within centimetres [2] and emitting on-axis betatron radiation as they oscillate [3,4]. For electrons with energy $\gamma m_e c^2$, the characteristics of the radiation are determined by the wiggler strength parameter $\alpha_\beta = \gamma k_\beta r_\beta$, where r_β is the amplitude and $k_\beta = 2\pi/\lambda_\beta$ is the wavenumber associated with betatron oscillations of wavelength λ_β. For self-injected electron bunches, where the accelerated electrons are swept up from the plasma itself, the parameter obeys $\alpha_\beta > 1$ and the radiation has the form of a broad band on-axis synchrotron spectrum [5,6] with a peak close to the critical energy

$$E_{\text{crit}} = \frac{3}{2}\hbar c \alpha_\beta k_\beta \gamma^2. \tag{1}$$

The number of photons can reach 10^{10} photons per pulse in a beam with 10 mrad divergence and critical energies in the range 10–50 keV [7,8], 10% stability [9] and pulse lengths of <100 fs [10,11].

The small size of the laser-driven accelerator is a key advantage compared to conventional synchrotron light sources and the technology has the potential to be used for a broad range of applications [1]. Tomographic imaging of biological samples [7,8,12,13], time resolved radiography of high energy density plasma [14] and imaging of AM objects [15] and complex microstructures [16] has been reported. The short pulse duration enables radiographic snapshots of fast moving parts with no motion blur. In addition, the source is suitable for x-ray absorption spectroscopy with exceptional time resolution [11]. Because the x-ray source size is of order of $2r_\beta \approx 1$ μm, high resolution imaging can be conducted with high x-ray flux, avoiding the trade off between source size and power encountered with conventional x-ray machines. Furthermore, within 1 m the beam has a transverse coherence length of 10's μm meaning that phase enhancement can be obtained with a compact imaging arrangement [17]. Phase contrast provides superior image quality for low density objects that only weakly attenuate x-rays and better distinction between items made of similar materials [18]. This technique has been demonstrated on biological samples using plasma based accelerators [17,19].

In this work, we demonstrate the feasibility of using laser-betatron radiation for high resolution NDE of industrially relevant components. The laser generates x-ray energies in the 10's keV range, ideal for low density polymer and carbon-fibre composite materials. We characterise the properties of the x-ray beams and present example images of

samples relevant to three particular areas of importance to industry: accurate metrology, battery development and composite manufacturing. We will discuss the potential of these sources for high frame rate industrial XCT as the underpinning laser technology develops to higher repetition rate operation in the next few years.

2. Imaging set-up and x-ray source

The beam line apparatus used to produce the x-ray beam can be seen in Fig. 1. The Gemini Ti:sapphire laser, providing pulses of duration 49 ± 3 fs and 7.2 ± 0.4 J on target, was focused with an off-axis $f/40$ parabola into a gas cell inside a vacuum chamber. Orthogonal to the main beam, a second laser pulse was used to measure the plasma electron density interferometrically. After the cell, the laser beam, electron beam and x-ray beam transited a 25 μm polyimide tape, which functioned as a plasma mirror deflecting most of the undepleted laser energy [20]. A 13 μm aluminium foil protected the sample from any remaining laser light and also acted to filter out 93% of the energy of a 14.6 keV-synchrotron spectrum below the k-edge (1.6 keV). Electrons were deflected off axis with a permanent magnetic dipole and observed on a scintillating screen to measure their energy spectrum. The x-ray beam exited the vacuum chamber through a 250 μm polyimide window and propagated through 2050 mm of air onto an indirect detection x-ray camera. This consisted of 150 μm thick caesium-iodide scintillator fibre-coupled to a 2048×2048 pixel CCD (Andor *iKon-L 936*) of pixel size 13.6 μm.

The gas cell length and gas pressure were scanned to determine the optimal parameters for generating stable x-ray beams. The most reproducible beams with the highest x-ray flux were measured at a plasma density of $4.4 \pm 0.4 \times 10^{18}$ cm^{-3} with an average peak energy of the electrons of 435 ± 7 MeV. The corresponding plasma wave wavelength λ_p implies a maximal x-ray pulse duration $\lambda_p/c \approx 50$ fs. The x-ray spectrum was measured using 12 materials in a filter pack configuration [21]. By comparing the transmission of the different materials relative to each other and finding the best fit synchrotron spectrum, the critical energy Eq. (1) was found to be 14.4 ± 1.4 keV for photons in the range $0.1 - 300$ keV. The emitted x-ray flux from the source was determined to be $5.2 \pm 1.7 \times 10^7$ photons mrad^{-2} per pulse and the transverse source
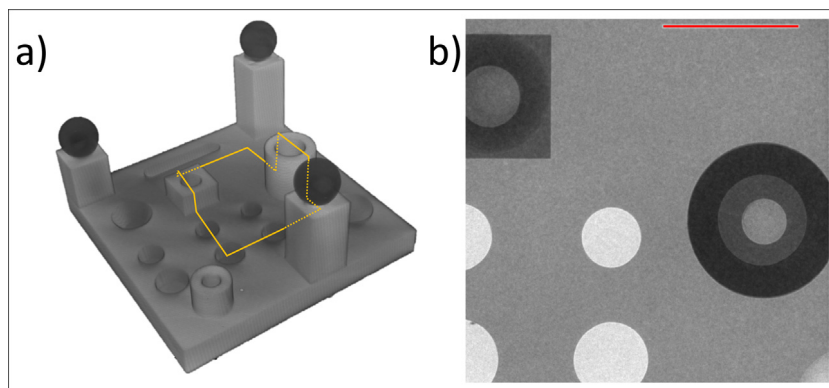
Fig. 2. Plastic test object with varying sphere diameters, external/internal diameters of cylinders, and plane to plane distances produced for XCT performance verification. (a) tomographic reconstruction using conventional lab x-ray CT (b) radiograph of the test object obtained with the laser-betatron source. The red line indicates 1 cm and the orange rectangle the field of the radiograph. (For interpretation of the references to colour in this figure legend, the reader is referred to the web version of this article.)
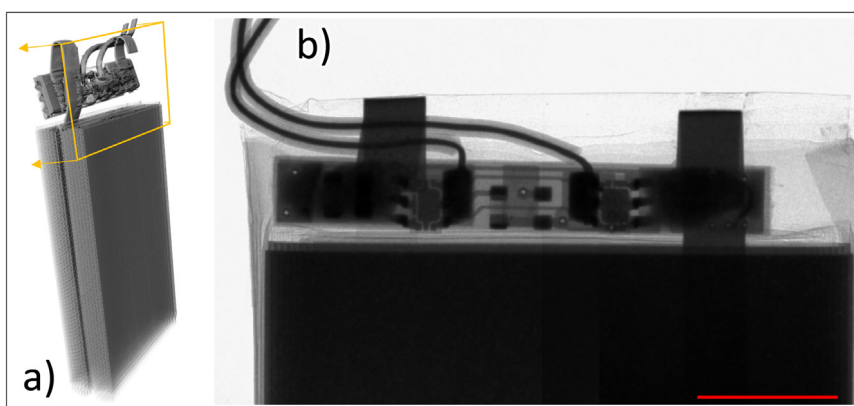

Fig. 3. (a) Tomographic reconstruction of a pouch cell obtained using conventional lab x-ray CT. Manufacturing defects can occur such as delamination of layers, improper electrode attachment, and poor welding in the tab area highlighted (b) Front view radiograph of the tab area obtained with the laser-betatron source. The red line indicates 1 cm. (For interpretation of the references to colour in this figure legend, the reader is referred to the web version of this article.)

size was inferred from the betatron parameters to be $2r_B = 2.3 \pm 0.3\,\mu m$ (Eq. (1)).

The divergence of the x-ray beam ($\sim 10\,mrad$) allows geometrical magnification. The beam line included three sample stages located at different distances in order to vary the x-ray field-of-view, as indicated in Fig. 1. Samples outside vacuum (position 3) could be positioned anywhere from the rear wall of the chamber to directly in front of the camera. Inside the vacuum chamber, a stage was placed close to the exit window (position 2) yielding a magnification $M = 2.2$, well suited for cm-scale objects. The highest magnification was $M = 10.2$ with the sample placed 370 mm from the source (position 1). Because this stage was located before the electron spectrometer magnet, an additional kicker magnet was inserted in this case to prevent the electron beam from striking the sample. The magnification was measured at position 1 using a JIMA *RT RC-02* resolution target and in configuration 2 using a gold foil with a pattern of horizontal and vertical apertures. The resulting radiographs are shown in Fig. 1.

Radiographs of industrial samples taken with the laser-betatron source are presented in Section 3. To provide context for each particular application, we also display 3D reconstructions of the same objects obtained using the commercial XCT scanners currently being used. In this work, it is not our intention to directly compare image quality between the x-ray sources. Rather, our aim is to demonstrate the capability for high quality imaging of such objects, with a view to offering advanced XCT using this technology in the future. The laser-betatron images in Figs. 2 and 3 were obtained with the samples placed outside the vacuum chamber with magnification of $M = 1.5$; the sample shown in Fig. 4 was imaged at position 2 ($M = 2.2$). The

image resolution was detector-limited by the point spread function of the scintillator to ($78\,\mu m\ /\ M$) [8]. For each acquisition 10 single x-ray images were integrated and an average flat field beam x-ray profile was background subtracted as well as a darkfield image. Clusters of hot pixels, due to bremsstrahlung, were removed using an adapted median filter, taking into account that bremsstrahlung affects multiple pixels.

3. Industrial applications

3.1. Dimensional XCT

Accurate metrology is a critical aspect of the manufacturing process to confirm that industrial components meet the required tolerances. This is particularly important for parts produced by AM, which have complicated internal structure that must be imaged in a non-destructive way. As an emerging technology, there is a need for new approaches to quality control and the definition of industry standards.[4]

Typical lab-based x-ray machines consisting of a cone beam have a plethora of measurement uncertainties in the scanning procedure. These include variations in operator selected parameters; geometric alignment of the system from the source, detector, and manipulator; and the environment [22]. Post-acquisition, the typical Feldkamp algorithm (FDK) [23] reconstruction introduces further error including approximations from the cone-beam. In an effort to assess the measurement uncertainty in industrial XCT, there have been studies to
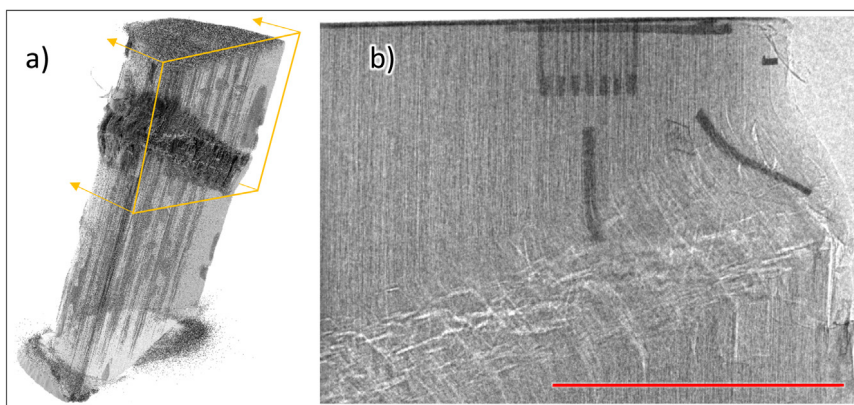
---

[4] amnationalstrategy.uk

Fig. 4. Kink band failure in a composite cylinder initiated by impact and propagated by compressive end loading. (a) tomographic reconstruction obtained using conventional lab x-ray CT (b) radiograph obtained with the laser-betatron source with carbon fibre tows visible. The red line indicates 1 cm. (For interpretation of the references to colour in this figure legend, the reader is referred to the web version of this article.)

understand the impact of various parameters and to evaluate performance [24–27]. Results from the entire process carried out on different machines in different locations have also been compared to assess consistency, as reported in numerous round robin tests [28–30].

An image using the laser-betatron source of a plastic test object produced for performance verification is shown in Fig. 2(b). These samples are made with a number of representative geometries designed to test the dimensional measurement accuracy of x-ray imaging systems. Dimensions such as sphere diameter, internal/external diameters of cylinders, centre-to-centre and plane-to-plane distances are typical examples of features that are assessed. In Fig. 2(a), a tomographic reconstruction of the sample is shown where these distances are evident in a 3D context. The accuracy and uncertainty of such a measurement is intrinsically linked to the quantity and quality of the data that can be captured. The radiograph displays exceptional sharpness with minimal noise due to the small source size and high photon count. This level of fidelity could potentially produce an unrivalled maximal permissible error across all measurements with sufficient radiographs and a high level of geometric calibration. The near-parallelism of the laser-betatron x-ray beam is beneficial as this limits imaging artefacts arising from cone beams. Additionally, the ability to tune the x-ray spectrum to higher energies would allow highly penetrating XCT of AM products made with dense materials such as super-alloys used in the automotive and aerospace sectors.

3.2. Battery technologies

Better understanding of electrochemical processes is essential to guide innovative product design enabling the transition to low-carbon technologies.[5] The manufacture of Li-batteries is in a constant state of development with new chemistries regularly being trialled, with assembly lines eventually needing to adapt. New processes are rarely right-first-time and can result in defects within the cell. While the manufacturing process is iterated, identification of these problems is paramount not only to maintain optimal performance but also for safety [31]. XCT is being exploited to investigate these issues but with manufacturing lines creating 6–10 cells per minute, a high speed solution is required if every cell is to be inspected.

The laser-betatron source is well suited to provide rapid NDE of battery components, as shown by the example image of a pouch cell in Fig. 3(b). Pouch cells consist of a gel layer, alternating between cathode and anode layers. The electrodes must be sufficiently separated with no contact between them to avoid shorting, and can also suffer from other manufacturing defects such as delamination. These individual layers

can be observed in a full tomographic reconstruction such as the one shown in Fig. 3(a). Another potential site for quality issues is the tab area visible at the top of the battery. This region is checked as part of a typical inspection process because poor welding of the tabs to the anode and cathode can result in a defective cell. The radiograph, centred on the tab area, highlights the quality achievable with the laser-betatron source, with phase enhancement aiding the distinction between components. For electrodes composed of weakly absorbing materials, such as graphite, phase imaging is necessary to achieve sufficient contrast [32].

Improvements in laser repetition rate will also enable *operando* XCT and time-resolved x-ray absorption spectroscopy (XAS) to examine the activity of battery cells during charge cycles. These methods allow visualisation of the changes in microstructure [32,33] and mapping of lithium concentration [34,35], important for understanding battery degradation. However, because of the very high average flux required, such studies can only be currently carried out using synchrotron light sources. A key advantage of the laser-produced x-ray pulse is its short duration and inherent synchronisation with the drive laser. The capability to measure ultrafast transitions would be particularly useful for pump-probe investigations on the femtosecond scale, for example studies of new photovoltaic materials [36]. Laser-betatron XAS measurements with $<100\,\mathrm{fs}$ temporal resolution have already been reported [11,37], demonstrating the suitability of the source for this application.

3.3. Composite manufacturing

To meet the huge rise in demand for composite products over a broad range of industries, it is essential to increase rates and efficiency in composite manufacturing.[6] NDE is commonly used to assess design features, test manufacturing methods, and inspect the effects of mechanical testing and damage that has occurred over the service lifetime of a part [38]. Detailed XCT information, along with finite element modelling [39], can improve efficiency through better design, and the definition of acceptance tolerances.

A major concern is the evolution of defects during manufacture. To be able to understand their formation, it is important to conduct *in-process* XCT to track individual features over time. This was highlighted by a study where samples were imaged with fast CT scans (7 min acquisition time) throughout the cure process inside the cabinet of an industrial scanner (Nikon *XTH-320*) [40]. The results showed that, although an initial gap between carbon fibre tows filled as the sample heated, small voids emerged that would affect the properties

---

of a finished product. This phenomenon was not detected in other studies using multiple partially cured samples [41], likely because of unavoidable variation in samples [42,43]. However, the long scan times necessary for high resolution and low noise images present difficulties for studies of fast changing samples. This is particularly true where the research requires distinguishing carbon fibre reinforcements from carbon-based polymer resins. Although this can be achieved with industrial scanners, scan times of order 4 h preclude this type of in-process XCT study. Synchrotron imaging can be adopted for uninterrupted in-situ studies, including mechanical tests of cured composite [44] and compression [45] and debulk [46] of uncured composite, but this is not a practical solution for regular use by industrial composite manufacturers because of availability and cost constraints.

These problems could be overcome by employing laser-driven x-ray sources. As an example, we show in Fig. 4(b) a radiograph, obtained with the laser-betatron source, of a composite test sample. This was a semi-circular prism cut from a cured cylinder made up from an array of small diameter unidirectional IM7 carbon fibre reinforced epoxy resin matrix rods, embedded in a second epoxy resin. XCT is used to assess the effect of a kink-band failure, initiated by impact and propagated by compressive end loading. This is visible in the tomographic reconstruction shown in Fig. 4(a). The radiograph exhibits good contrast between the carbon fibre and the resin, highlighting the benefit of the x-ray phase enhancement produced with the laser-betatron source. The layers visible in the image are carbon fibre tows that typically have a diameter of order $200\,\mu m$. Development of this technology to deliver fast scanning at high resolution would address larger scale challenges, such as imaging consolidation in corners, or inspecting full scale parts while applying heat, vacuum and/or pressure to the part. In this way, quality assurance and control could be performed before the heat and pressure is applied to cure the resin, reducing scrap, and saving energy, cost and time.

4. Discussion

The demands of state-of-the-art industrial NDE, such as high resolution, fast scan speed and element specific analysis, are difficult to meet with existing x-ray technology. Laser-based radiation sources produced with a plasma accelerator have ideal properties for addressing these challenges. Recent improvements in reliability and repetition rate of high power lasers make it feasible to produce these compact x-ray devices for commercial deployment in industrial environments. At the laser energy used here of 7 J (125 TW laser power), commercial products are available operating at 5 Hz (e.g. Thales *Quark200*; Amplitude *Pulsar*) and would increase the average x-ray flux to above $10^{11}\,\mathrm{ph\,s^{-1}}$. Using diode-pumped solid state technology the repetition rate could be scaled up further [47–50]. Improvements in x-ray beam consistency have been demonstrated by reducing pulse-to-pulse fluctuations in the laser and gas target performance [51] and through studies of the stability of electron injection mechanisms into the accelerator [9]. Using higher power drive lasers [6,52], the photon energy should be enhanced to the 100's keV to MeV range that will be needed for inspection of large battery packs and full-scale composite products such as wind turbines, although this also increases the size and cost of the system. The laser requirements might be relaxed by adapting target design to increase the betatron photon energy [53].

One of the benefits of adopting laser-driven technology is the ability to drive different, synchronised secondary sources with the same laser. Moderate adaptations to the system can produce other particles that can be utilised for complementary sub-surface inspection techniques such as neutron imaging [54] and positron annihilation lifetime spectroscopy [55]. Therefore, a single machine could be used to deliver a powerful inspection capability with multi-modal, multi-scale imaging.

To be viable as a commercial product, considerable R & D effort is needed to ensure robust performance over long periods and to minimise the size and cost of the system. Product design could be tailored to meet the specific demands of the end-user, with a range of systems dependent on space and budget constraints. The compact design of modern high power lasers means that it would also be possible to integrate them into portable devices [56]. An important consideration is the radiation shielding necessary for the electron beam. In an industrial environment this could be constructed in a similar way to free-electron laser and synchrotron facilities where the electron beam is deflected into a heavily shielded beam dump in the ground while the x-ray beam propagates into an end-station with relatively light shielding.

Although a product based on this technology would be more costly and complex than conventional x-ray machines, it would offer advanced NDE tools that are currently not available in industrial or lab-based settings. In particular, micron-scale resolution tomography with fast scan speed, and ultrafast x-ray absorption spectroscopy could be applied to in situ inspection and product development. For example, using a laser operating at 100 Hz, high frame rate imaging of metre-scale objects should be possible at less than 1 min per square metre. Hard x-ray chemical tomography could also be conducted following the methods used on XAS synchrotron beamlines [57].

Declaration of competing interest

The authors declare that they have no known competing financial interests or personal relationships that could have appeared to influence the work reported in this paper.

References

[1] F. Albert, A.G.R. Thomas, Plasma physics and controlled fusion vol 1, Plasma Phys. Control. Fusion 58 (103001) (2016).

[2] K. Poder, M. Tamburini, G. Sarri, A.D. Piazza, S. Kuschel, C.D. Baird, K. Behm, S. Bohlen, J.M. Cole, D.J. Corvan, M. Duff, E. Gerstmayr, C.H. Keitel, K. Krushelnick, S.P.D. Mangles, P. McKenna, C.D. Murphy, Z. Najmudin, C.P. Ridgers, G.M. Samarin, D.R. Symes, A.G.R. Thomas, J. Warwick, M. Zepf, Experimental signatures of the quantum nature of radiation reaction in the field of an ultraintense laser, Phys. Rev. X 8 (031004) (2018).

[3] A. Rousse, K. Ta Phuoc, R. Shah, A. Pukhov, E. Lefebvre, V. Malka, S. Kiselev, F. Burgy, J.P. Rousseau, D. Umstadter, D. Hulin, Production of a keV Xray beam from synchrotron radiation in relativistic laser-plasma interaction, Phys. Rev. Lett. 93 (13) (2004) 135005.

[4] S. Kneip, C. McGuffey, J.L. Martins, S.F. Martins, C. Bellei, V. Chvykov, F. Dollar, R.A. Fonseca, C. Huntington, G. Kalintchenko, A. Maksimchuk, S.P.D. Mangles, T. Matsuoka, S.R. Nagel, C.A.J. Palmer, J. Schreiber, K.T. Phuoc, A.G.R. Thomas, V. Yanovsky, L.O. Silva, K. Krushelnick, Z. Najmudin, Bright spatially coherent synchrotron X-rays from a table-top source, Nat. Phys. 6 (12) (2010) 980–983.

[5] E. Esarey, B.A. Shadwick, P. Catravas, W.P. Leemans, Synchrotron radiation from electron beams in plasma-focusing channels, Phys. Rev. E 65 (5) (2002) 1–15.

[6] A.G.R. Thomas, Scalings for radiation from plasma bubbles, Phys. Plasmas 17 (5) (2010) 056708.

[7] J.M. Cole, J.C. Wood, N.C. Lopes, K. Poder, R.L. Abel, S. Alatabi, J.S.J. Bryant, A. Jin, S. Kneip, K. Mecseki, S. Parker, D.R. Symes, M.A. Sandholzer, S.P.D. Mangles, Z. Najmudin, Tomography of human trabecular bone with a laser-wakefield driven x-ray source, Plasma Phys. Control. Fusion 58 (1) (2016) 014008.

[8] J.M. Cole, D.R. Symes, N.C. Lopes, J.C. Wood, K. Poder, S. Alatabi, S.W. Botchway, P.S. Foster, S. Gratton, S. Johnson, C. Kamperidis, O. Kononenko, M. De Lazzari, C.A.J. Palmer, D. Rusby, J. Sanderson, M. Sandholzer, G. Sarri, Z. Szoke-Kovacs, L. Teboul, J.M. Thompson, J.R. Warwick, H. Westerberg, M.A. Hill, D.P. Norris, S.P.D. Mangles, Z. Najmudin, High-resolution μCT of a mouse embryo using a compact laser-driven X-ray betatron source., Proc. Natl. Acad. Sci. USA 115 (25) (2018) 6335–6340.

[9] A. Döpp, B. Mahieu, A. Lifschitz, C. Thaury, A. Doche, E. Guillaume, G. Grittani, O. Lundh, M. Hansson, J. Gautier, M. Kozlova, J.P. Goddet, P. Rousseau, A. Tafzi, V. Malka, A. Rousse, S. Corde, K. Ta Phuoc, Stable femtosecond X-rays with tunable polarization from a laser-driven accelerator, Light: Sci. Appl. 6 (11) (2017) e17086.

[10] K. Ta Phuoc, R. Fitour, A. Tafzi, T. Garl, N. Artemiev, R. Shah, F. Albert, D. Boschetto, A. Rousse, D.E. Kim, A. Pukhov, V. Seredov, I. Kostyukov, Demonstration of the ultrafast nature of laser produced betatron radiation, Phys. Plasmas 14 (8) (2007) 080701.

[11] B. Mahieu, N. Jourdain, K. Ta Phuoc, F. Dorchies, J.-P. Goddet, A. Lifschitz, P. Renaudin, L. Lecherbourg, Probing warm dense matter using femtosecond X-ray absorption spectroscopy with a laser-produced betatron source, Nature Commun. 9 (1) (2018) 3276.

[12] J. Wenz, S. Schleede, K. Khrennikov, M. Bech, P. Thibault, M. Heigoldt, F. Pfeiffer, S. Karsch, Quantitative X-ray phase-contrast microtomography from a compact laser-driven betatron source, Nature Commun. 6 (May) (2015) 1–6.

[13] A. Döpp, L. Hehn, J. Götzfried, J. Wenz, M. Gilljohann, H. Ding, S. Schindler, F. Pfeiffer, S. Karsch, Quick x-ray microtomography using a laser-driven betatron source, Optica 5 (2) (2018) 199.

[14] J.C. Wood, D.J. Chapman, K. Poder, N.C. Lopes, M.E. Rutherford, T.G. White, F. Albert, K.T. Behm, N. Booth, J.S. Bryant, P.S. Foster, S. Glenzer, E. Hill, K. Krushelnick, Z. Najmudin, B.B. Pollock, S. Rose, W. Schumaker, R.H. Scott, M. Sherlock, A.G. Thomas, Z. Zhao, D.E. Eakins, S.P. Mangles, Ultrafast imaging of laser driven shock waves using betatron X-rays from a laser wakefield accelerator, Sci. Rep. 8 (1) (2018) 11010.

[15] M. Vargas, W. Schumaker, Z.-H. He, K. Behm, V. Chvykov, B. Hou, K. Krushelnick, A. Maksimchuk, J.A. Nees, V. Yanovsky, Z. Zhao, A.G.R. Thomas, X-ray phase contrast imaging of additive manufactured structures using a laser wakefield accelerator, Plasma Phys. Control. Fusion 61 (5) (2019) 54009.

[16] A.E. Hussein, N. Senabulya, Y. Ma, M.J. Streeter, B. Kettle, S.J. Dann, F. Albert, N. Bourgeois, S. Cipiccia, J.M. Cole, O. Finlay, E. Gerstmayr, I.G. González, A. Higginbotham, D.A. Jaroszynski, K. Falk, K. Krushelnick, N. Lemos, N.C. Lopes, C. Lumsdon, O. Lundh, S.P. Mangles, Z. Najmudin, P.P. Rajeev, C.M. Schlepütz, M. Shahzad, M. Smid, R. Spesyvtsev, D.R. Symes, G. Vieux, L. Willingale, J.C. Wood, A.J. Shahani, A.G. Thomas, Laser-wakefield accelerators for high-resolution X-ray imaging of complex microstructures, Sci. Rep. 9 (1) (2019) 3249.

[17] S. Kneip, C. McGuffey, F. Dollar, M.S. Bloom, V. Chvykov, G. Kalintchenko, K. Krushelnick, A. Maksimchuk, S.P. Mangles, T. Matsuoka, Z. Najmudin, C.A. Palmer, J. Schreiber, W. Schumaker, A.G. Thomas, V. Yanovsky, X-ray phase contrast imaging of biological specimens with femtosecond pulses of betatron radiation from a compact laser plasma wakefield accelerator, Appl. Phys. Lett. 99 (9) (2011) 1–4.

[18] M. Stampanoni, A. Groso, A. Isenegger, G. Mikuljan, Q. Chen, A. Bertrand, S. Henein, R. Betemps, U. Frommherz, P. Böhler, D. Meister, M. Lange, R. Abela, Trends in synchrotron-based tomographic imaging: the SLS experience, in: Developments in X-Ray Tomography V, Vol. 6318, 2006, 63180M–63180M–14.

[19] S. Fourmaux, S. Corde, K.T. Phuoc, P. Lassonde, G. Lebrun, S. Payeur, F. Martin, S. Sebban, V. Malka, A. Rousse, J.C. Kieffer, Single shot phase contrast imaging using laser-produced betatron x-ray beams, Opt. Lett. 36 (13) (2011) 2426.

[20] C. Thaury, F. Quéré, J.-P. Geindre, A. Levy, T. Ceccotti, P. Monot, M. Bougeard, F. Réau, P. D'Oliveira, P. Audebert, R. Marjoribanks, P. Martin, Plasma mirrors for ultrahigh-intensity optics, Nat. Phys. 3 (6) (2007) 424–429.

[21] S. Kneip, S.R. Nagel, C. Bellei, N. Bourgeois, A.E. Dangor, A. Gopal, R. Heathcote, S.P. Mangles, J.R. Marquès, A. Maksimchuk, P.M. Nilson, K.T. Phuoc, S. Reed, M. Tzoufras, F.S. Tsung, L. Willingale, W.B. Mori, A. Rousse, K. Krushelnick, Z. Najmudin, Observation of synchrotron radiation from electrons accelerated in a petawatt-laser-generated plasma cavity, Phys. Rev. Lett. 100 (10) (2008) 1–4.

[22] J.P. Kruth, M. Bartscher, S. Carmignato, R. Schmitt, L. De Chiffre, A. Weckenmann, Computed tomography for dimensional metrology, CIRP Ann. 60 (2) (2011) 821–842.

[23] L.A. Feldkamp, L.C. Davis, J.W. Kress, Practical cone-beam algorithm, J. Opt. Soc. Amer. A 1 (6) (1984) 612–619.

[24] R. Schmitt, C. Niggemann, Uncertainty in measurement for x-ray-computed tomography using calibrated work pieces, Meas. Sci. Technol. 21 (5) (2010) 054008.

[25] J. Kumar, A. Attridge, P.K. Wood, M.A. Williams, Analysis of the effect of cone-beam geometry and test object configuration on the measurement accuracy of a computed tomography scanner used for dimensional measurement, in: Measurement Science and Technology, Vol. 22, (3) Institute of Physics Publishing, 2011.

[26] P. Müller, J. Hiller, A. Cantatore, L. De Chiffre, A study on evaluation strategies in dimensional x-ray computed tomography by estimation of measurement uncertainties, Int. J. Metrol. Qual. Eng. 3 (2) (2012) 107–115.

[27] J. Hiller, M. Maisl, L.M. Reindl, Physical characterization and performance evaluation of an x-ray micro-computed tomography system for dimensional metrology applications, Meas. Sci. Technol. 23 (8) (2012) 085404.

[28] S. Carmignato, Accuracy of industrial computed tomography measurements: Experimental results from an international comparison, CIRP Ann.. 61 (1) (2012) 491–494.

[29] J.A.B. Angel, L. De Chiffre, E. Larsen, J. Rasmussen, R. Sobiecki, General rights inter laboratory comparison on industrial computed tomography CIA-CT comparison. Reference measurements CIA-ct_reference_measurements_01 CIA-CT comparison inter laboratory comparison on industrial computed tomography reference measurements list of contents, in: Inter Laboratory Comparison on Industrial Computed Tomography: CIA-CT Comparison. Reference Measurements. DTU Mechanical Engineering. CIA-CT Reference Measurements, Tech. Rep., (01) DTU Mechanical Engineering, APA, 2013.

[30] A. Townsend, R. Racasan, R. Leach, N. Senin, A. Thompson, A. Ramsey, D. Bate, P. Woolliams, S. Brown, L. Blunt, An interlaboratory comparison of X-ray computed tomography measurement for texture and dimensional characterisation of additively manufactured parts, Addit. Manuf. 23 (2018) 422–432.

[31] M. Loveridge, G. Remy, N. Kourra, R. Genieser, A. Barai, M. Lain, Y. Guo, M. Amor-Segan, M. Williams, T. Amietszajew, M. Ellis, R. Bhagat, D. Greenwood, Looking deeper into the galaxy (note 7), Batteries 4 (1) (2018) 3.

[32] P. Pietsch, D. Westhoff, J. Feinauer, J. Eller, F. Marone, M. Stampanoni, V. Schmidt, V. Wood, Quantifying microstructural dynamics and electrochemical activity of graphite and silicon-graphite lithium ion battery anodes, Nature Commun. 7 (1) (2016) 12909.

[33] M. Ebner, F. Marone, M. Stampanoni, V. Wood, Visualization and quantification of electrochemical and mechanical degradation in Li ion batteries, Science 342 (6159) (2013) 716–720.

[34] L. Nowack, D. Grolimund, V. Samson, F. Marone, V. Wood, Rapid mapping of lithiation dynamics in transition metal oxide particles with operando X-ray absorption spectroscopy, Sci. Rep. 6 (1) (2016) 21479.

[35] J. Wang, Y.-c. Karen Chen-Wiegart, C. Eng, Q. Shen, J. Wang, Visualization of anisotropic-isotropic phase transformation dynamics in battery electrode particles, Nature Commun. 7 (1) (2016) 12372.

[36] Y. Uemura, D. Kido, A. Koide, Y. Wakisaka, Y. Niwa, S. Nozawa, K. Ichiyanagi, R. Fukaya, S.-i. Adachi, T. Katayama, T. Togashi, S. Owada, M. Yabashi, K. Hatada, A. Iwase, A. Kudo, S. Takakusagi, T. Yokoyama, K. Asakura, Capturing local structure modulations of photoexcited BiVO$_4$ by ultrafast transient XAFS, Chem. Commun. 53 (53) (2017) 7314–7317.

[37] B. Kettle, E. Gerstmayr, M. Streeter, F. Albert, R. Baggott, N. Bourgeois, J. Cole, S. Dann, K. Falk, I. Gallardo González, A. Hussein, N. Lemos, N. Lopes, O. Lundh, Y. Ma, S. Rose, C. Spindloe, D. Symes, M. Šmíd, A. Thomas, R. Watt, S. Mangles, Single-shot multi-keV X-ray absorption spectroscopy using an ultrashort laser-wakefield accelerator source, Phys. Rev. Lett. 123 (25) (2019) 254801.

[38] S.C. Garcea, Y. Wang, P.J. Withers, X-ray computed tomography of polymer composites, Compos. Sci. Technol. 156 (2018) 305–319.

[39] J.P.-H. Belnoue, T. Mesogitis, O.J. Nixon-Pearson, J. Kratz, D.S. Ivanov, I.K. Partridge, K.D. Potter, S.R. Hallett, Understanding and predicting defect formation in automated fibre placement pre-preg laminates, Composites A 102 (2017) 196–206.

[40] L.R. Pickard, K. Smith, J. Kratz, K. Potter, Tracking the evolution of a defect, characteristic of afp layup, during cure with in-process micro-ct scanning, in: 21st International Conference on Composite Materials, 2017.

[41] L.R. Pickard, Towards Efficient Composites Manufacture Through In-Process Monitoring and Knowledge Management (Dissertation), University of Bristol, 2019.

[42] T. Centea, P. Hubert, Measuring the impregnation of an out-of-autoclave prepreg by micro-CT, Compos. Sci. Technol. 71 (5) (2011) 593–599.

[43] L. Serrano, Systèmes époxyde- Cuisson hors autoclave et basse température (Ph.D. thesis), Université de Toulouse, 2018.

[44] A.E. Scott, M. Mavrogordato, P. Wright, I. Sinclair, S.M. Spearing, In situ fibre fracture measurement in carbon–epoxy laminates using high resolution computed tomography, Compos. Sci. Technol. 71 (12) (2011) 1471–1477.

[45] D.F. Sentis, L. Orgéas, P.J.J. Dumont, S.R. du Roscoat, M. Sager, P. Latil, 3D in situ observations of the compressibility and pore transport in sheet moulding compounds during the early stages of compression moulding, Composites A 92 (2017) 51–61.

[46] J. Thompson, et al., ''Micro-Computed Tomographic Synchrotron Techniques for Non-destructive Testing of out of Autoclave Composite Materials, '' in Design, manufacturing and applications of composites, in: Tenth Joint Canada-Japan Workshop on Composites, 2014, pp. 331–335.

[47] P. Mason, M. Divoký, K. Ertel, J. Pilař, T. Butcher, M. Hanuš, S. Banerjee, J. Phillips, J. Smith, M.D. Vido, A. Lucianetti, C. Hernandez-Gomez, C. Edwards, T. Mocek, J. Collier, Kilowatt average power 100 J-level diode pumped solid state laser, Optica 4 (4) (2017) 438–439.

[48] C.L. Haefner, A. Bayramian, S. Betts, R. Bopp, S. Buck, J. Cupal, M. Drouin, A. Erlandson, J. Horáček, J. Horner, J. Jarboe, K. Kasl, D. Kim, E. Koh, L. Koubíková, W. Maranville, C. Marshall, D. Mason, J. Menapace, P. Miller, P. Mazurek, A. Naylon, J. Novák, D. Peceli, P. Rosso, K. Schaffers, E. Sistrunk, D. Smith, T. Spinka, J. Stanley, R. Steele, C. Stolz, T. Suratwala, S. Telford, J. Thoma, D. VanBlarcom, J. Weiss, P. Wegner, High average power, diode pumped petawatt laser systems: a new generation of lasers enabling precision science and commercial applications, in: G. Korn, L.O. Silva (Eds.), Proceedings Volume 10241, Research using Extreme Light: Entering New Frontiers with Petawatt-Class Lasers III, Vol. 10241, International Society for Optics and Photonics, 2017, 1024102.

[49] L. Gizzi, P. Koester, L. Labate, F. Mathieu, Z. Mazzotta, G. Toci, M. Vannini, A viable laser driver for a user plasma accelerator, Nucl. Instrum. Methods Phys. Res. A 909 (2018) 58–66.

[50] W.P. Leemans, Report of Workshop on Laser Technology for k-BELLA and Beyond, Lawrence Berkeley National Laboratory, 2017, Workshop held at Lawrence Berkeley National Laboratory.

[51] N. Delbos, C. Werle, I. Dornmair, T. Eichner, L. Hübner, S. Jalas, S.W. Jolly, M. Kirchen, V. Leroux, P. Messner, M. Schnepp, M. Trunk, P.A. Walker, P. Winkler, A.R. Maier, LUX – A laser–plasma driven undulator beamline, Nucl. Instrum. Methods Phys. Res. A 909 (2018) 318–322.

[52] S. Kneip, Z. Najmudin, A.G.R. Thomas, A plasma wiggler beamline for 100 TW to 10 PW lasers, High Energy Density Phys. 8 (2) (2012) 133–140.

[53] J. Ferri, S. Corde, A. Döpp, A. Lifschitz, A. Doche, C. Thaury, K. Ta Phuoc, B. Mahieu, I.A. Andriyash, V. Malka, X. Davoine, High-brilliance betatron γ -ray source powered by laser-accelerated electrons, Phys. Rev. Lett. 120 (25) (2018) 254802.

[54] E. Lehmann, D. Mannes, A. Kaestner, C. Grünzweig, Recent applications of neutron imaging methods, Physics Procedia 88 (September 2016) (2017) 5–12.

[55] M. Butterling, W. Anwand, T.E. Cowan, A. Hartmann, M. Jungmann, R. Krause-Rehberg, A. Krille, A. Wagner, Gamma-induced positron spectroscopy (GiPS) at a superconducting electron linear accelerator, Nucl. Instrum. Methods Phys. Res. B 269 (22) (2011) 2623–2629.

[56] H. Wille, M. Rodriguez, J. Kasparian, D. Mondelain, J. Yu, A. Mysyrowicz, R. Sauerbrey, J.P. Wolf, L. Wöste, Teramobile: A mobile femtosecond-terawatt laser and detection system, Eur. Phys. J. AP 20 (2002) 183–190.

[57] S.W.T. Price, K. Ignatyev, K. Geraki, M. Basham, J. Filik, N.T. Vo, P.T. Witte, A.M. Beale, J.F.W. Mosselmans, Chemical imaging of single catalyst particles with scanning μ-XANES-CT and μ-XRF-CT, Phys. Chem. Chem. Phys. 17 (1) (2015) 521–529.